THE FRACTIONAL STEP METHOD APPLIED TO SIMULATIONS OF NATURAL CONVECTIVE FLOWS

Douglas G. Westra
NASA Marshall Space Flight Center

Dr. Juan C. Heinrich
Professor, Aerospace and Mechanical Engineering Department, University of Arizona

ABSTRACT

This paper describes research done to apply the Fractional Step Method to finite-element simulations of natural convective flows in a directionally solidified metal alloy casting.

The Fractional Step Method (FSM), also known as the projection method and as the splitting method, has been applied commonly to high Reynolds number flow simulations, but is less common for low Reynolds number flows, such as natural convection in permeable media. The FSM offers increased speed and reduced memory requirements by allowing the non-coupled solution of the pressure and the velocity components.

The FSM is expected to offer significant benefits for predicting flows in a directionally solidified alloy, since other methods presently employed are not efficient. Previously, the most suitable finite-elements based method for predicting flow in a directionally solidified binary alloy has been the penalty method. The penalty method has the disadvantage that it requires the coupled solution of the velocity components using direct matrix solvers, due to the penalty term. The FSM allows the decoupled iterative solution of the finite element equations, thereby greatly increasing the efficiency of the method. The FSM also lends itself to parallel processing, since the velocity component stiffness matrices can be built and solved independently of each other.

Numerical simulations are now commonly used to predict macrosegregation in directionally solidified castings. In particular, the finite-element simulations can predict the existence of "channels" within the processing mushy zone and subsequently "freckles" within the fully processed solid, which are known to result from macrosegregation, due to thermosolutal convection of the melt during the solidification process. Freckles cause strong material non-uniformities in the castings that are therefore scrapped.

The phenomena of natural and thermosolutal convection in an alloy undergoing directional solidification will be explained. The momentum and continuity equations for natural convection in a fluid, a permeable medium, and in a binary alloy undergoing directional solidification will be presented. Finally, results for natural convection in a pure liquid, natural convection in a medium with a constant permeability, and for a fluid layer overlying a mushy zone solidifying directionally will be presented.

INTRODUCTION

Natural convection occurs in many physical situations. Its most common occurrence arises from thermal gradients skewed to the direction of gravity in a gas or liquid. Thermally driven natural convection can also occur in permeable media. Density driven natural convection also occurs in more complex situations, such as in a liquid metal alloy undergoing directional solidification. In the latter case, the force that drives the fluid motion stems from a combination of density differences driven by thermal and concentration gradients in the liquid, and is referred to as thermosolutal convection.

The ultimate goal of the work described here is to develop a mathematical model and subsequently the capability to simulate the fluid flow occurring in a directionally solidifying alloy, using the fractional step method. The fundamental equations describing flow in a directionally solidifying alloy are complicated. In addition, implementation of the FSM is challenging. For this reason, the FSM is first applied to the two-dimensional equations governing natural convection in a single-phase fluid that can be treated as containing a single constituent. Next, the FSM is applied to the equations governing natural convection in a permeable medium, containing a single-phase fluid of one constituent. Finally, the FSM is applied to the equations governing natural convection in a binary alloy undergoing directional solidification.

This paper is laid out as follows. The next section discusses the phenomena occurring in a directional solidifying alloy that contribute to convection, and the need to understand these flows. Then fundamentals of the FSM are discussed, followed by the application of the FSM to the equations governing flow in a fluid and in permeable media. Results of simulations for these two different flow situations are presented and discussed next. Then the FSM as applied to the equations governing flow in a binary alloy undergoing directional solidification is presented. Finally, results of simulations for this flow situation are presented and discussed.

DIRECTIONAL SOLIDIFICATION

DEFECTS IN ALLOYS AND THEIR CAUSES

The directional solidification process is used to produce aircraft engine turbine blades. Casting defects often necessitate that the entire casting be scrapped, which is very costly. A major defect that leads to scrapped castings is that of concentration non-uniformities. These are a direct result of the fluid motion that takes place in the melt during the solidification process, and affects the consistency and integrity of the casting's structural properties. Segregation that produces concentration non-uniformities is classified under microsegregation or macrosegregation, depending on the length scale. Microsegregation is a phenomenon that occurs over a distance approaching the size of the primary dendrite arm space and depends on the shape of the dendrites and solute diffusion in the mushy zone [1,2,3]. Macrosegregation involves compositional differences over distances approaching that of the size of the casting or ingot; it is due to convection in the melt, and is large in scale compared to that caused by diffusion.

During vertical directional solidification, the casting is cooled from below. This inhibits convection by imposing a stable temperature gradient. Strictly speaking, due to the stability impressed on the melt by cooling it from below, it is expected that thermal convection will be mostly suppressed. However, because of the partitioning of the solute constituents at the solidifying interface, density gradients due to differential solute concentrations are generated in the interdendritic liquid that interact with the temperature field and trigger convection [4,5,6]. This combination of phenomena is often referred to as thermosolutal or double-diffusive convection. Thermosolutal convection is often the main cause of severe macrosegregation in castings.

One of the most perverse macrosegregation defects is "freckles", which are caused by convection. These defects are made up of long narrow streaks oriented roughly parallel to the direction of gravity. Freckles have solute concentrations that vary significantly from that of the surroundings [7]. The freckles make the casting prone to fatigue cracking at the interfaces. Therefore, the castings are scrapped. Several experimental works with nonmetallic transparent systems [8,9,10] have verified this.

PRESENT SIMULATION CAPABILITIES

Previous research, related to the one proposed herein, as described in References [11,12,13,14,15] has come a long way in simulation of solidification processes. The models currently used include interdendritic diffusion, thermosolutal convection, and solute and energy conservation. Since the mushy zone is an assembly of dendrites of complicated morphology, it is modeled as a region of anisotropic permeability with no predetermined size or shape [16].

Presently, the size of the domains that can be simulated is limited because of the large amount of computer resources required. This limitation is attributed mainly to two issues: 1) In order to adequately capture the diffusion processes occurring in the mushy zone, very fine meshes are required, on the order of the primary dendrite arm spacing, and 2) since permeability theory is used to model the varying liquid fraction of the mushy zone, the only numerical algorithms that have been successfully employed to solve the momentum equation stiffness matrix use direct matrix solvers.

When discretizing using finite element models, the penalty method is presently the algorithm employed most frequently for the solution of the solidification momentum equation stiffness matrices. The pressure is not calculated directly in the penalty method formulation. Rather, the pressure term is eliminated by equivalencing it to the continuity equation (which, numerically, has a value very near zero) times a very large penalty parameter [17]. All velocity components are calculated simultaneously at each time step. Therefore, for a three-dimensional finite-element computation domain consisting of N nodes, the momentum equation stiffness matrix has a size of order 3N X 3N. The stiffness matrix generated by the penalty method requires direct matrix solvers, due to the numerical stiffness introduced by the penalty term and due to the permeability term [11,12].

The computer resources required by mixed formulations are even more than for the penalty method, since the matrices generated by a mixed formulation are non-symmetric [17]. The pressure is calculated with no approximations; therefore there are four unknowns per node, making the stiffness matrix size of order 4N X 4N. Since direct formulations characteristically produce very large ill-formed stiffness matrices, direct formulations are normally used only for calibration of the penalty and other methods [11].

The Galerkin-Least-Squares method was used in the 3D computations described in References [15,18], and allowed for simulations in somewhat larger domains. However, this method is also restricted and very difficult to use.

The attractive feature of the FSM is that the velocity components and the pressure can be de-coupled and solved independently. This leads to stiffness matrices that are much smaller and therefore much more manageable. In fact, it makes it possible to perform simulations in much larger domains that were previously prohibitive. The FSM is described next.

FUNDAMENTAL PRINCIPLES OF THE FRACTIONAL STEP METHOD

The FSM has been used extensively for solution of the incompressible Navier-Stokes equations in Computational Fluid Dynamics (CFD). Chorin [19,20,21] introduced the method over thirty years ago and Temam [22] independently developed similar ideas. A general description of its implementation is discussed here.

Beginning with the dimensionless form of the incompressible Navier-Stokes equation and continuity:

$$\frac{\mathbf{u}_{n+1}-\mathbf{u}_n}{\Delta t}-\frac{1}{\mathrm{Re}}\nabla^2\mathbf{u}_{n+1}=-\nabla p_{n+1}-\mathbf{u}_n\cdot\nabla\mathbf{u}_n+\mathbf{f}_n \tag{1.1}$$

$$\nabla\cdot\mathbf{u}=0 \tag{1.2}$$

where the velocity has been discretized in time, the viscous and pressure terms are treated implicitly and the convective and forcing term $\mathbf{f}_n$ are treated explicitly. This equation is split into two steps, the intermediate "viscous" step:

$$\frac{\tilde{\mathbf{u}}_{n+1}-\mathbf{u}_n}{\Delta t}-\frac{1}{\mathrm{Re}}\nabla^2\tilde{\mathbf{u}}_{n+1}=-\mathbf{u}_n\cdot\nabla\mathbf{u}_n+\mathbf{f}_n \tag{1.3}$$

and the projection or "inviscid" step:

$$\frac{\mathbf{u}_{n+1}-\tilde{\mathbf{u}}_{n+1}}{\Delta t}-\frac{1}{\mathrm{Re}}\nabla^2\left(\mathbf{u}_{n+1}-\tilde{\mathbf{u}}_{n+1}\right)=-\nabla p_{n+1} \tag{1.4}$$

Taking the divergence of equation (1.4) and dropping the term $\frac{1}{\mathrm{Re}}\nabla^2\tilde{\mathbf{u}}_{n+1}$, the equation for the pressure is obtained.

$$\nabla^2 p_{n+1} = \frac{\nabla\cdot\tilde{\mathbf{u}}_{n+1}}{\Delta t} \tag{1.5}$$

The reason most often cited for removing this term is that the intermediate velocity profile is projected into an "inviscid" vector space, orthogonal to the intermediate "viscous" space [23,24]. Some references treat the viscous term explicitly [25] in equation (1.3) so that it does not appear in equation (1.4). However, explicit treatment of the viscous term restricts numerical stability, particularly for low Reynolds number flows. Other references include a more mathematically pure derivation [26,27]. In these references, the FSM derived above is modified as follows: The pressure in equation (1.4) is replaced with $p = \psi - \frac{\Delta t}{\mathrm{Re}}\nabla^2\psi$:

$$\frac{\mathbf{u}_{n+1}-\tilde{\mathbf{u}}_{n+1}}{\Delta t} - \frac{1}{\mathrm{Re}}\nabla^2\left(\mathbf{u}_{n+1}-\tilde{\mathbf{u}}_{n+1}\right) = -\nabla\left(\psi_{n+1} - \frac{\Delta t}{\mathrm{Re}}\nabla^2\psi_{n+1}\right) \tag{1.6}$$

The following terms are removed from equation (1.6) to take on the same form as equation (1.4), without the implicit viscous term:

$$\frac{\mathbf{u}_{n+1}-\tilde{\mathbf{u}}_{n+1}}{\Delta t} = -\nabla\psi_{n+1} \tag{1.7}$$

Applying the Laplace operator to equation (1.7), multiplying both sides by $\frac{\Delta t}{\mathrm{Re}}$, and substituting into equation (1.6) reduces equation (1.6) to equation (1.7). Therefore, removing these terms is mathematically correct.

Taking the divergence of equation (1.7) yields a Poisson equation for ψ instead of p:

$$\nabla^2\psi_{n+1} = \frac{\nabla\cdot\tilde{\mathbf{u}}_{n+1}}{\Delta t} \tag{1.8}$$

and the pressure at the end of the time step is calculated as:

$$p_{n+1} = \psi_{n+1} - \frac{\Delta t}{\mathrm{Re}}\nabla^2\psi_{n+1} \tag{1.9}$$

Whether calculating the pressure from equations (1.6), (1.8), and (1.9) is more accurate than calculating it directly from equations (1.4) and (1.5) is application dependent and must be tested in practice [26].

THE ACCURACY OF THE FRACTIONAL STEP METHOD

A number of authors have predicted the accuracy of the FSM for incompressible flow [26-29]. The general consensus is that the velocity can be determined to second-order accuracy. However, there is disagreement on pressure. Some claim the pressure can be determined to second order accuracy [30,31], while others claim that the very nature of the FSM limits the pressure to first-order accuracy no matter what steps are taken to improve the method [28,29]. Fortunately, there is consistent agreement on how to improve its accuracy.

The three main methods of ensuring acceptable accuracy for the FSM are:

1) Accurate selection of boundary conditions for the intermediate velocity as suggested by Kim and Moin [32].
2) Accurate selection of boundary conditions for the pressure as suggested by Orszag et al. [33] and E. and Liu [24,34].
3) The use of pressure-correction schemes as demonstrated by Van Kan [31], Bell et al. [30], Quartapelle [25], and Gresho [35,36].

The first two items hint at one of the inherent stumbling blocks of the FSM [28]. That is, there is only one set of the "real" boundary conditions: the boundary condition for the divergence-free velocity. Since the splitting of the Navier-Stokes equations into two steps requires two sets of boundary conditions, one must be very careful in setting up these boundary conditions.

The third item substitutes the calculation of the pressure at every time step with an "incremental" pressure calculation. That is, the pressure is adjusted or corrected at every time step relative to the previous time step's pressure.

MATHEMATICAL MODEL FOR NATURAL CONVECTION: WITH AND WITHOUT PERMEABILITY

The developments of the equations for the solution of Navier-Stokes equations for natural convection in a single-phase, single-constituent fluid and in a permeable medium are very similar. The only difference is the permeability term. Therefore, the development of the equations for a permeable medium is developed here. The equations for natural convection in a fluid can be obtained by removing the permeability term.

DEVELOPMENT OF DIMENSIONLESS MOMENTUM EQUATION FOR NATURAL CONVECTION IN A PERMEABLE MEDIUM

Using the Brinkman and Boussinesq approximations [37-39], the equations of motion for a fluid layer overlying a porous medium are:

Momentum:

$$\rho_0\left(\frac{\partial \mathbf{u}'}{\partial t'}+\mathbf{u}'\cdot\nabla'\mathbf{u}'\right)=-\nabla' p'+\mu\nabla'^2\mathbf{u}'-\mu\left(\mathbf{K}'\right)^{-1}\mathbf{u}'+\rho\,\mathbf{g}' \tag{2.1}$$

and Continuity:

$$\nabla'\cdot\mathbf{u}'=0 \tag{2.2}$$

where the permeability tensor $\mathbf{K}'$ is defined from the Darcy equation [40]:

$$\mathbf{u}'=-\frac{\mathbf{K}'}{\mu}\left(\nabla' p'-\rho\,\mathbf{g}'\right) \tag{2.3}$$

The primes indicate dimensional terms. Equation (2.1) shows the permeability term as a tensor to account for its anisotropy. For the analysis described in this section, **K** is assumed to be isotropic, therefore the permeability term will be shown as a scalar term.

For convenience, the components of the hydrostatic pressure (based on the reference density) are separated from the pressure:

$$p'=p'^{*}+\rho_0\left(g'_x x'+g'_y y'\right) \tag{2.4}$$

where p'^{*} is a modified pressure, and the reference density ρ_0 is defined as the density of the fluid at $T = T_0$. The gradient of the pressure can be written as:

$$\nabla' p'=\nabla' p'^{*}+\rho_0\,\mathbf{g}' \tag{2.5}$$

The linear Boussinesq approximation gives $\rho=\rho_0\left[1+\beta_T\left(T'-T'_0\right)\right]$. After substituting equation (2.5), the dimensional momentum equation becomes:

$$\frac{\partial \mathbf{u}'}{\partial t'}+\mathbf{u}'\cdot\nabla'\mathbf{u}'=-\frac{1}{\rho_0}\nabla' p'^{*}+\nu\nabla'^2\mathbf{u}'-\nu K^{-1}\mathbf{u}'+\beta_T\left(T'-T'_0\right)\mathbf{g}'$$

The equations are non-dimensionalized according to the following reference variables:

$$
\begin{aligned}
&\textit{Characteristic Length } H \\
&\textit{Characteristic Velocity } V = \sqrt{\beta_T\, g\, \Delta T\, H} \\
&x = \frac{x'}{H}, \quad y = \frac{y'}{H}, \quad \mathbf{u} = \frac{\mathbf{u}'}{V} \\
&p^* = \frac{p'^*}{p_0^*} \quad \textit{where} \quad p_0^* = \frac{\rho_0 D_T^2}{H^2} \\
&\nabla = \nabla' H \qquad Da = \frac{K}{H^2} \\
&\hat{\mathbf{g}} = \frac{\mathbf{g}'}{g} \qquad T = \frac{T' - T_0'}{\Delta T} \\
&t = \frac{t'}{\tau} \quad \textit{where} \quad \tau = \frac{H^2}{D_T}
\end{aligned}
\tag{2.6}
$$

For convenience, drop the * from p and organize according to the following dimensionless parameters:

$$
\begin{aligned}
&\textit{The Rayleigh Number}: \quad Ra_T = \frac{\beta_T\, g\, \Delta T\, H^3}{\nu D_T}, \\
&\textit{The Prandtl Number}: \quad Pr = \frac{\nu}{D_T}
\end{aligned}
\tag{2.7}
$$

This results in the dimensionless momentum equation:

$$
\frac{1}{\sqrt{\mathrm{Pr}\,\mathrm{Ra_T}}}\frac{\partial \mathbf{u}}{\partial t} + \mathbf{u}\cdot\nabla\mathbf{u} = -\frac{1}{\mathrm{Pr}\,\mathrm{Ra_T}}\nabla p + \sqrt{\frac{\mathrm{Pr}}{\mathrm{Ra_T}}}\nabla^2\mathbf{u} - \sqrt{\frac{\mathrm{Pr}}{\mathrm{Ra_T}}}\mathrm{Da}^{-1}\,\mathbf{u} + \mathrm{T}\,\hat{\mathbf{g}} \tag{2.8}
$$

The dimensionless continuity equation has the same form as the dimensional version:

$$
\nabla\cdot\mathbf{u} = 0 \tag{2.9}
$$

APPLICATION OF THE FRACTIONAL STEP METHOD TO THE MOMENTUM EQUATION FOR NATURAL CONVECTION IN A PERMEABLE MEDIUM

In order to build stable stiffness matrices for the finite element method, equation (2.8) is rearranged to treat the viscous term and permeability term implicitly and all other terms are moved to the right hand side to be treated explicitly. The FSM requires that the transient term be discretized, therefore the subscripts n and n+1 are added, where n refers to the value at the previous time step (known) and n+1 refers to the value at the present time step (unknown).

$$\frac{\mathbf{u}_{n+1}-\mathbf{u}_n}{\Delta t\sqrt{\mathrm{Pr}\,\mathrm{Ra}_T}}+\sqrt{\frac{\mathrm{Pr}}{\mathrm{Ra}_T}}\mathrm{Da}^{-1}\,\mathbf{u}_{n+1}-\sqrt{\frac{\mathrm{Pr}}{\mathrm{Ra}_T}}\nabla^2\mathbf{u}_{n+1}=-\frac{1}{\mathrm{Pr}\,\mathrm{Ra}_T}\nabla p_{n+1}-\mathbf{u}_n\cdot\nabla\mathbf{u}_n+T_n\,\hat{\mathbf{g}} \quad (2.10)$$

This is rearranged to the following:

$$\frac{1}{\Delta t\sqrt{\mathrm{Pr}\,\mathrm{Ra}_T}}\left(1+\Delta t\,\mathrm{Pr}\,\mathrm{Da}^{-1}-\Delta t\,\mathrm{Pr}\,\nabla^2\right)\mathbf{u}_{n+1}=-\frac{1}{\mathrm{Pr}\,\mathrm{Ra}_T}\nabla p_{n+1}+\mathbf{f}_n \quad (2.11)$$

where the forcing term $\mathbf{f}_n=-\mathbf{u}_n\cdot\nabla\mathbf{u}_n+T_n\,\hat{\mathbf{g}}+\frac{1}{\Delta t\sqrt{\mathrm{Pr}\,Ra_T}}\mathbf{u}_n$.

Use the equality $p_{n+1}=p_n+\left(p_{n+1}-p_n\right)$ to calculate the incremental pressure at every time step. Equation (2.11) then becomes:

$$\frac{1}{\Delta t\sqrt{\mathrm{Pr}\,Ra_T}}\left(1+\Delta t\,\mathrm{Pr}\,Da^{-1}-\theta\,\Delta t\,\mathrm{Pr}\,\nabla^2\right)\mathbf{u}_{n+1}=-\frac{\left[\nabla p_n+\nabla\left(p_{n+1}-p_n\right)\right]}{\mathrm{Pr}\,Ra_T}+\mathbf{f}_n \quad (2.12)$$

Split Equation (2.12) into a intermediate (viscous) step and a projection (inviscid) step, respectively:

$$\frac{1}{\Delta t\sqrt{\mathrm{Pr}\,Ra_T}}\left(1+\Delta t\,\mathrm{Pr}\,Da^{-1}-\Delta t\,\mathrm{Pr}\,\nabla^2\right)\tilde{\mathbf{u}}_{n+1}=-\frac{1}{\mathrm{Pr}\,Ra_T}\nabla p_n+\mathbf{f}_n \quad (2.13)$$

$$\frac{1}{\Delta t\sqrt{\mathrm{Pr}\,Ra_T}}\left(1+\Delta t\,\mathrm{Pr}\,Da^{-1}-\Delta t\,\mathrm{Pr}\,\nabla^2\right)\left(\mathbf{u}_{n+1}-\tilde{\mathbf{u}}_{n+1}\right)=-\frac{1}{\mathrm{Pr}\,Ra_T}\nabla\left(p_{n+1}-p_n\right) \quad (2.14)$$

where $\tilde{\mathbf{u}}_{n+1}$ is the solution to the intermediate step and does not satisfy continuity. Now, take the divergence of the projection step, equation (2.14)

$$\frac{1}{\Delta t\sqrt{\mathrm{Pr}\,Ra_T}}\nabla\cdot\left\{\left(1+\Delta t\,\mathrm{Pr}\,Da^{-1}-\Delta t\,\mathrm{Pr}\,\nabla^2\right)\left(\mathbf{u}_{n+1}-\tilde{\mathbf{u}}_{n+1}\right)\right\}=-\frac{1}{\mathrm{Pr}\,Ra_T}\nabla^2\left(p_{n+1}-p_n\right) \quad (2.15)$$

Note that at the end of the time step, the velocity must satisfy continuity, therefore the divergence of both $\mathbf{u}_{n+1}$ and $\nabla^2\,\mathbf{u}_{n+1}$ are 0 and the intermediate viscous term is ignored, resulting in

$$\nabla^2\left(p_{n+1}-p_n\right)=\frac{\sqrt{Pr\,Ra_T}}{\Delta t}\left(1+\Delta t\,Pr\,Da^{-1}\right)\nabla\cdot\tilde{\mathbf{u}}_{n+1} \quad (2.16)$$

To find the divergence-free velocity at the end of the time step, solve for each component of velocity from equation (2.14), with the viscous term ignored.

$$u_{n+1} = \tilde{u}_{n+1} - \frac{1}{\left(1 + \Delta t\, Pr\, Da^{-1}\right)} \frac{\Delta t}{\sqrt{Pr\, Ra_T}} \frac{\partial}{\partial x}\left(p_{n+1} - p_n\right) \tag{2.17}$$

$$v_{n+1} = \tilde{v}_{n+1} - \frac{1}{\left(1 + \Delta t\, \mathrm{Pr}\, Da^{-1}\right)} \frac{\Delta t}{\sqrt{\mathrm{Pr}\, Ra_T}} \frac{\partial}{\partial y}\left(p_{n+1} - p_n\right) \tag{2.18}$$

For a pure liquid, the permeability term K and its dimensionless counter-part Da approach infinity, therefore K^{-1} and Da^{-1} approach zero and are eliminated from the above equations. In order to solve the above equations numerically, the finite element method is applied using the Galerkin formulation. For details on how the Galerkin finite element method is formulated the reader should consult references [17,41].

RESULTS FOR SIMULATIONS OF NATURAL CONVECTION OF A FREE FLUID AND OF A FLUID IN A PERMEABLE MEDIUM

Figures 1 – 6 show steady-state results of the fractional step method applied to the simulation of Rayleigh-Bénard flow in a pure liquid and in a permeable medium. Figures 1 – 5 are contour plots of the temperature with the velocity vectors superimposed. Figure 6 is a contour plot of the pressure for the same case as Figure 5. There are 41 nodes in each direction in all cases. The results are presented in dimensionless form; the dimensionless temperature is 1.0 at the bottom and 0.0 at the top. The gravity vector is oriented in the negative y-direction to create an unstable thermal condition. The gravity vector has a magnitude of 9.81 m/s^2 in all simulations. Table I summarizes these results, listing the dimensionless parameters defined in equation (2.7). Fluid properties are given, along with appropriate scaling parameters that correspond to the Rayleigh Numbers and Prandtl Numbers listed. In two of the cases, fluid properties of air and water at 300 K were used. The reference variables relate to physical dimensions, boundary conditions, and fluid properties through equation (2.6). The results are in excellent agreement with results obtained for the same cases using the penalty function formulation.

THE FRACTIONAL STEP METHOD APPLIED TO THE MOMENTUM EQUATION FOR DIRECTIONAL SOLIDIFICATION IN A BINARY ALLOY

The above formulation demonstrates the process of applying the FSM to a single-constituent, single-phase fluid, with and without permeability. Directional solidification of a binary alloy is much more complicated. This process includes two constituents, two phases and an anisotropic permeability. Developing the formulation here would require considerable space. Therefore, only the results of the formulation are presented. Please consult [11] for more details.

The simulation of directional solidification in a binary alloy includes conservation of energy, species, mass, and momentum balance. Since the FSM affects only the conservation of mass and momentum balance, only those equations are presented here. Please consult [11,42,43] for more details regarding the equations for conservation of energy and species.

The dimensionless equation for momentum balance in a directionally solidifying binary alloy is [11]:

$$\frac{\partial \mathbf{u}}{\partial t}+\frac{\phi}{\mathrm{Re}}\mathbf{Da}^{-1}\mathbf{u}-\frac{1}{\mathrm{Re}}\nabla^2\mathbf{u}=-\phi\nabla p-\frac{1}{\phi}\mathbf{u}\cdot\nabla\mathbf{u}$$
$$-\frac{\beta}{\phi}\frac{\partial\phi}{\partial t}\mathbf{u}+\frac{\beta}{3\,\mathrm{Re}}\nabla\frac{\partial\phi}{\partial t}+\phi\left[\frac{\mathrm{Ra_T}}{\mathrm{Re^2\,Pr}}T+\frac{\mathrm{Ra_S}}{\mathrm{Re^2\,Sc}}\left(S_L-1\right)\right]\hat{\mathbf{g}} \tag{3.1}$$

and the continuity equation is

$$\nabla\cdot\mathbf{u}=\beta\frac{\partial\phi}{\partial t}. \tag{3.2}$$

where β is the shrinkage coefficient and is defined as $\beta=\dfrac{\rho_s-\rho_l}{\rho_l}$.

The momentum equation, equation (3.1) is split up into two steps in order to be solved using the FSM. The dimensionless equation for the intermediate step is:

$$\frac{1}{\Delta t}\left(1+\frac{\phi\,\Delta t}{\mathrm{Re}}\mathbf{Da}^{-1}\right)\tilde{\mathbf{u}}_{n+1}-\frac{1}{\mathrm{Re}}\nabla^2\tilde{\mathbf{u}}_{n+1}=\mathbf{f}_n-\phi\nabla p_n \tag{3.3}$$

where the (explicit) forcing term $\mathbf{f}_n$ is defined as

$$\mathbf{f}_n=-\frac{1}{\phi}\mathbf{u}_n\cdot\nabla\mathbf{u}_n-\frac{\beta\,\Delta t}{\phi}\frac{\partial\phi}{\partial t}+\frac{\beta}{3\,\mathrm{Re}}\nabla\frac{\partial\phi}{\partial t}+\phi\left[\frac{\mathrm{Ra_T}}{\mathrm{Re^2\,Pr}}T+\frac{\mathrm{Ra_S}}{\mathrm{Re^2\,Sc}}\left(S_L-1\right)\right]\hat{\mathbf{g}}+\frac{\mathbf{u}_n}{\Delta t} \tag{3.4}$$

The dimensionless equation for the projection step is

$$\frac{1}{\Delta t}\left(1+\frac{\phi\,\Delta t}{\mathrm{Re}}\mathbf{Da}^{-1}\right)\left(\mathbf{u}_{n+1}-\tilde{\mathbf{u}}_{n+1}\right)-\frac{1}{\mathrm{Re}}\nabla^2\left(\mathbf{u}_{n+1}-\tilde{\mathbf{u}}_{n+1}\right)=-\phi\nabla\left(p_{n+1}-p_n\right) \tag{3.5}$$

The implicit viscous term is ignored and continuity is imposed by taking the divergence of equation (3.5)

$$\nabla\cdot\left[\boldsymbol{\sigma}\nabla\left(p_{n+1}-p_n\right)\right]=\frac{\nabla\cdot\tilde{\mathbf{u}}_{n+1}}{\Delta t}-\frac{\beta}{\Delta t}\frac{\partial\phi}{\partial t} \tag{3.6}$$

where the dimensionless term $\boldsymbol{\sigma}$ is a function of the fraction liquid ϕ and the anisotropic Darcy term and is a vector quantity,

$$\boldsymbol{\sigma} = \begin{pmatrix} \sigma_x & 0 \\ 0 & \sigma_y \end{pmatrix} \tag{3.7}$$

where the individual components of $\boldsymbol{\sigma}$ are as defined by Sabau, et al. [44].

$$\sigma_x = \frac{\phi}{1 + \dfrac{\phi\,\Delta t}{\mathrm{Re}\,\mathrm{Da}_x}}, \text{ and } \sigma_y = \frac{\phi}{1 + \dfrac{\phi\,\Delta t}{\mathrm{Re}\,\mathrm{Da}_y}} \tag{3.8}$$

The dimensionless scaling parameters are:

$$\begin{aligned}
&\text{The Reynold's Number:} && \mathrm{Re} = \frac{VH}{\nu} \\
&\text{The Thermal Rayleigh Number:} && \mathrm{Ra}_T = \frac{\beta_T g G H^4}{\nu D_T} \\
&\text{The Solute Rayleigh Number:} && \mathrm{Ra}_S = \frac{\beta_S g S_0 H^3}{\nu D_S} \\
&\text{The Prandtl Number:} && \mathrm{Pr} = \frac{\nu}{D_T} \\
&\text{The Schmidt Number:} && \mathrm{Sc} = \frac{\nu}{D_S}
\end{aligned} \tag{3.9}$$

RESULTS FOR SIMULATIONS OF CONVECTION IN A BINARY ALLOY UNDERGOING DIRECTIONAL SOLIDIFICATION

Figure 7 shows the simulation domain, which is an 0.008 m by 0.03 m rectangle, for an alloy comprised of Pb-5.8% wt. Sb. A mesh spacing of 0.0002 m is used, which is on the order of the primary dendrite arm spacing. The initial condition consists of a fixed temperature at the bottom boundary (Y' = 0) set to the alloy liquidus temperature and an imposed thermal gradient of G_0 = 12,000 K/m (positive with respect to Y') throughout the liquid melt. The liquid melt is of uniform composition S_0 = 5.8 wt% Sb. The simulated boundary conditions are an imposed thermal gradient of 12,000 K/m at the top boundary, and 0.36 K/s cooling at the bottom (the temperature at the bottom boundary is changed in time). A uniform body force of 9.81 m/s^2 is imposed in the negative Y'-direction. Figure 7(a) shows the three zones that are normally present during solidification: liquid, solid, and mush.

Figures 8 – 11 show transient simulation results of the FSM applied to the momentum equation for natural convection in a binary alloy undergoing directional solidification. In this case, the

boundary condition is continually changing and there is no steady state. The simulated time is 400 seconds in Figures 8 – 12.

Figure 8 shows the temperature and pressure, clearly indicating the imposed temperature gradient and the resulting pressure gradient. Figure 9 shows a plot of the fraction liquid and the concentration of the alloy throughout. The three regions are labeled on the left hand side of Figure 9: "Liquid, "Mush" or mushy zone, and "Solid". At this solidification time, the mushy zone is located approximately between Y = 0.007 and 0.010 meters. The "freckles" on the concentration plot are clearly seen and are a result of thermosolutal convection. The distortion of the fraction liquid from a purely vertical gradient is also obvious and is a direct result of the thermosolutal convection. Figure 10 shows the same plot of fraction liquid and concentration as in Figure 9, with the velocity vectors super-imposed. It is seen that the velocities emanate from the regions of highest deviation from the base concentration of S_0. Figure 11 shows a close-up of the velocities and concentration occurring just above the mushy zone. Finally, Figure 12 shows the velocities and concentration occurring in the mushy zone. The code is achieving acceptable continuity when simulating velocities even in the mushy zone, where the magnitude of the velocity is several orders of magnitude smaller than the velocities occurring in the all-liquid region. These results also agree very well with those obtained using the penalty finite element formulation.

CONCLUSION

Natural convection is a phenomenon that occurs in free moving fluids, fluids contained in permeable media, and in alloys undergoing solidification. Thermosolutal convection in castings that are being directionally solidified leads to concentration non-uniformities that result in scrapping the castings. The FSM has been successfully applied to simulations involving a binary alloy undergoing directional solidification. It is expected that in simulations of directional solidification the FSM will allow us to greatly increase the size of the domains to be simulated. The results presented here are for two-dimensional domains only. However, the results are highly encouraging and efforts are now underway to extend simulation of directional solidification with the fractional step method to three dimensions.

REFERENCES

[1] Kurz, W. and Fisher, D.J. "Fundamentals of Solidification". Trans Tech Publications. 1992.

[2] Porter, D.A. and Easterling, K.E. "Phase Transformations in Metals and Alloys, Second Edition." Chapman & Hall. 1992.

[3] Flemings, MC. "Solidification processing". McGraw-Hill, New York, NY. 1974.

[4] Favier J.J. "Recent advances in Bridgman growth modeling and fluid flow." *Journal of Crystal Growth* **99**: 18-29 (1990).

[5] Rouzaud A, Camel D, and Favier JJ. "A comparative study of thermal and thermosolutal convective effects in vertical Bridgman crystal growth." *Journal of Crystal Growth* **73**: 149-166 (1985).

[6] Nandapurkar P., Poirier D.R., Heinrich J.C., and Felicelli S. "Thermosolutal Convection during Dendritic Solidification of Alloys: Part I. Linear Stability Analysis", *Metallurgical Material Transactions B. Numer.* **20B**: 711-721 (1989).

[7] Sarazin JR and Hellawell A. "Channel formation in Pb-Sn, Pb-Sb and Pb-Sb-Ab alloy ingots and comparisons with the system NH_4Cl-H_20." *Metallurgical Material Transactions A.* **19A**: 1861-1871 (1988).

[8] Copley SM, Giamei AF, Johnson SM and Hornbecker MF. *Metallurgical Material Transactions.* **1**: 2193-2204 (1970).

[9] Chen F, and Chen CF. *J .Fluid Mech.* **227**: 567-586 (1991).

[10] Sample A and Hellawell A. "The effect of mold precision in channel and macrosegregation in ammonium chloride water analog castings." *Metallurgical Material Transactions B.* **13B**: 495-501 (1982).

[11] Heinrich JC and McBride E. "Calculation of pressure in the mushy zone", *Int. J. Numer. Methods Engng.* 47, 735-747 (2000).

[12] McBride E, Heinrich JC, and Poirier DR. "Numerical simulation of incompressible flow driven by density variations during phase change." *Int. J. Numer. Methods in Fluids* **31**: 787-800 (1999).

[13] Felicelli SD, Poirier DR and Heinrich JC. "Finite element analysis of directional solidification of multi-component alloys", *Int. J. Numer. Methods in Fluids* **27**: 207-227 (1998).

[14] Heinrich JC, Felicelli S, Nandapurkar P, and Poirier DR. "Thermosolutal Convection during Dendritic Solidification of Alloys: Part II. Nonlinear Convection", *Metallurgical Material Transactions B.* **20B**: 883-891 (1989).

[15] Felicelli SD, Heinrich J.C., and Poirier D.R. "Three-dimensional simulations of freckles in binary alloys." *Journal of Crystal Growth* **191**: 879-888 (1998).

[16] Felicelli SD, Poirier DR, and Heinrich JC. "Simulation of Freckles during Vertical Solidification of Binary Alloys." *Metallurgical Material Transactions B. Numer.* **22B**: 847-859 (1991).

[17] Heinrich JC, and Pepper DW. "Intermediate Finite Element Method, Fluid Flow and Heat Transfer Applications." Taylor & Francis. 1999.

[18] Felicelli SD, Poirier DR and Heinrich JC. "Modeling freckle formation in three dimensions during solidification of multi-component alloys" *Metallurgical Material Transactions B*. **29B**: 847-855 (1998).

[19] Chorin AJ "The numerical solution of the Navier-Stokes equations for an incompressible fluid." *Bull. Amer. Math Soc*. **73**: 928-931 (1967).

[20] Chorin AJ "Numerical solution of the Navier-Stokes equations." *Math Comp*. **22**: 745-762 (1968).

[21] Chorin AJ "On the convergence of discrete approximations to the Navier-Stokes equations." *Math Comp.* **23**: 341-353 (1969).

[22] Temam R. "Sur l'approximation de la solution des equations de Navier-Stokes par la mehode des fractionnarires II. *Arch. Rational Mech Anal*. **33**: 377-385 (1969).

[23] Almgren AS, Bell JB, and Szymczak WG. "A numerical method for the incompressible Navier-Stokes Equations based on an approximate projection." *SIAM J. Sci. Comput*. **17, No. 2**: 358-369 (1996).

[24] E W and Liu J-G. "Projection method I: Convergence and numerical boundary layers." *SIAM Journal of Numerical Analysis*. **32**: 1017-1057 (1995).

[25] Quartapelle L. "Numerical Solution of the Incompressible Navier-Stokes Equations." Birkhauser Verlag, Berlin. 1993.

[26] Shen J. "On error estimates of projection methods for Navier-Stokes equations: First-order schemes. *SIAM J. Numer. Anal*. **29**: 57-77 (1992).

[27] Shen J. "On error estimates of some higher order projection and penalty-projection methods for Navier-Stokes equations: First-order schemes. *Numer. Math*. **62**: 49-73 (1992).

[28] Strikwerda JC and Lee YS. "The accuracy of the fractional-step method". *SIAM Journal of Numerical Analysis*. **37, No. 1**: 37-47 (1999).

[29] Perot JB. "An analysis of the fractional step method." *J. Comput. Phys*. **108**: 51-58 (1993).

[30] Bell JB, Colella P, and Glaz HM. "A second-order projection method for the incompressible Navier-Stokes equations." *J. Comput. Phys*. **85**: 257-283 (1989).

[31] Van Kan J. "A second-order accurate pressure-correction scheme for viscous incompressible flow." *SIAM J. Sci. Stat. Comput*. **7**: 870-891 (1986).

[32] Kim J, and Moin P. Application of a fractional-step method to incompressible Navier-Stokes." *J. Comput. Phys*. **59**: 308-323 (1985).

[33] Orszag SA, Israeli M, and Deville MO. "Boundary conditions for incompressible flows." *Journal of Scientific Computing*. **1**: 75-110. (1986).

[34] E W and Liu J-G. "Projection method II: Godunov-Ryabenki analysis." *SIAM Journal of Numerical Analysis*. **33**: 1597-1621 (1996).

[35] Gresho PM. "On the theory of semi-implicit projection methods for viscous incompressible flow and its implementation via a finite element method that also introduces a nearly consistent mass matrix. Part 1: Theory." *Int. J. for Numer. Methods in Fluids*. **11**: 587-620 (1990).

[36] Gresho PM and Chan ST. "On the theory of semi-implicit projection methods for viscous incompressible flow and its implementation via a finite element method that also introduces a nearly consistent mass matrix. Part 2: Implementation." *Int. J. for Numer. Methods in Fluids*. **11**: 621-659 (1990).

[37] Beavers GS and Joseph DD. "Boundary conditions at a naturally permeable wall." *J. Fluid Mech.* **30**: 197-207 (1967).

[38] Nield DA. "The boundary correction for the Rayleigh-Darcy problem: limitations of the Brinkman problem." *J. Fluid Mech.* **128**: 37-46 (1982).

[39] Chandrasekhar S. "Hydrodynamic and hydromagnetic stability." Dover Publications, Inc. New York. 1961.

[40] Bird RB, Stewart WE, and Lightfoot EN. "Transport Phenomena." John Wiley, New York, NY, 1960, pp. 59 and 150.

[41] Pepper DW, and Heinrich JC. "The Finite Element Method, Basic Concepts and Applications." Taylor & Francis. 1992.

[42] Ganesan S and Poirier DR. "Conservation of mass and momentum for the flow of interdendritic liquid during solidification." *Metall. Trans.* **21B**: 173-181 (1993).

[43] Poirier DR, Nandapurkar PJ, and Ganesan S. "The energy and solute conservation equations for dendritic solidification." *Metall. Trans.* **22B**: 889-900 (1991).

[44] Sabau AS, Han Q, and Viswanathan S. "Projection Methods for Interdendritic Flows." 128th TMS Annual Meeting & Exhibition. San Diego. 1999.

CONTACT

Douglas G. Westra
NASA / Marshall Space Flight Center
Mail Code ED25
MSFC, AL 35812

(256) 544-3120 (256) 544-0800 (FAX)
doug.westra@msfc.nasa.gov

NOMENCLATURE

Scalars

β	shrinkage coefficient due to phase change from liquid to solid
β_T	coefficient of thermal expansion, 1/K
β_S	coefficient of solute expansion
ρ_0	reference density, kg/m^3
ρ_L	density of liquid, kg/m^3
ρ_S	density of solid, kg/m^3
ϕ	fraction liquid
μ	dynamic viscosity, N-s/m^2
ν	kinematic viscosity, m^2/s
ψ	pressure function, Pa
D_T	thermal diffusivity, m^2/s
D_S	solute diffusivity, m^2/s
g	value of gravity vector, m/s^2
G	reference thermal gradient, K/m
H	reference length, m
p’	pressure, Pa
p'^*	modified pressure, Pa
Pr	Prandtl Number
Re	Reynolds Number

Ra_T thermal Rayleigh Number

Ra_S solute Rayleigh Number

Sc Schmidt Number

S_0 reference solute concentration, %

t' time, s

Δt time step size, s

T' temperature, K

ΔT reference temperature difference, K

u' velocity in x direction, m/s

v' velocity in y direction, m/s

V reference velocity, m/s

Vectors and Tensors

Da permeability, dimensionless

K permeability , m^2

g gravity vector, m/s^2

n direction normal to boundary

t' direction tangent to boundary

u' velocity vector, m/s

Table I

Scaling Parameters, Reference Variables, and Fluid Properties for Figures 1- 6

Figure	Ra	Pr	Da	ΔT [a] (K)	Fluid Properties	H [a] (m)	V [a] (m/s)
1	10^5	1.00	N/A	100	See Note b	1.0	0.32
2	10^5	7.00	N/A	100	See Note c	1.0	0.26
3	10^6	0.71	N/A	85	**Air @ 300 K**	0.05	0.38
4	10^6	1.0	10^{-4}	100	See Note d	1.0	0.31
5, 6	10^8	5.83	10^{-6}	20	**Water @ 300 K**	0.06	0.06

a - Reference Variables given in equation (2.6).

b - The thermal coefficient of expansion is assumed to be –0.0001 K^{-1}, the kinematic viscosity is assumed to be 10^{-3} m^2/s, and the thermal diffusivity is assumed to be 10^{-3} m^2/s.

c - The thermal coefficient of expansion is assumed to be –0.0001 K^{-1}, the kinematic viscosity is assumed to be 7 X 10^{-4} m^2/s, and the thermal diffusivity is assumed to be 10^{-4} m^2/s.

d - The thermal coefficient of expansion is assumed to be –0.001 K^{-1}, the kinematic viscosity is assumed to be 10^{-3} m^2/s, and the thermal diffusivity is assumed to be 10^{-3} m^2/s .

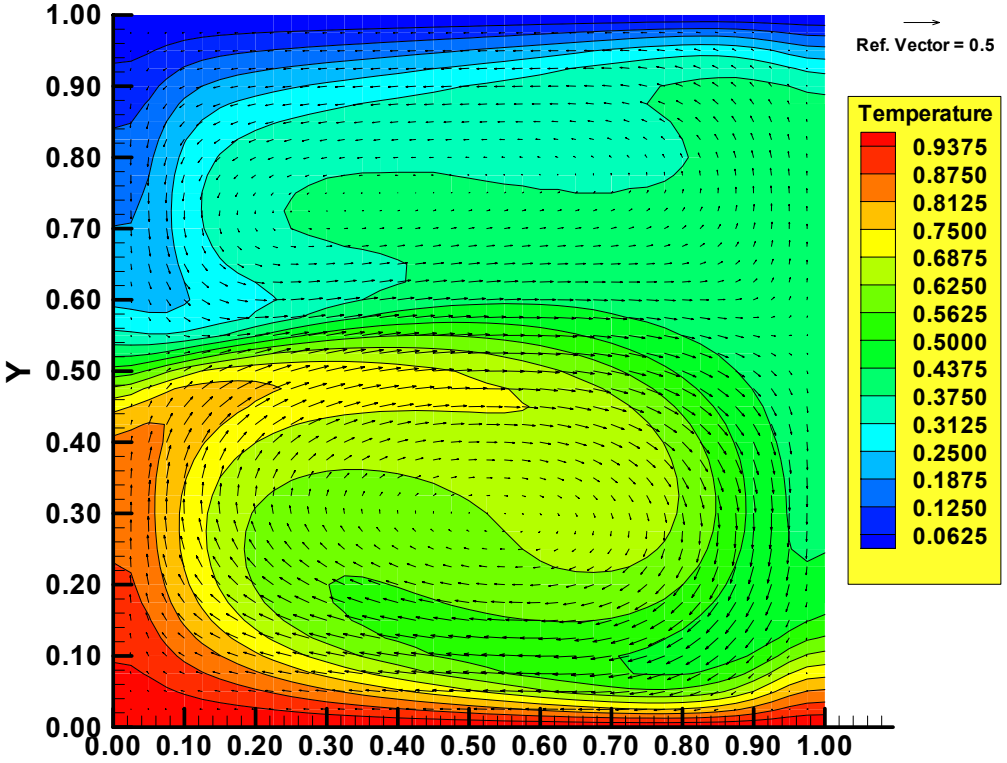

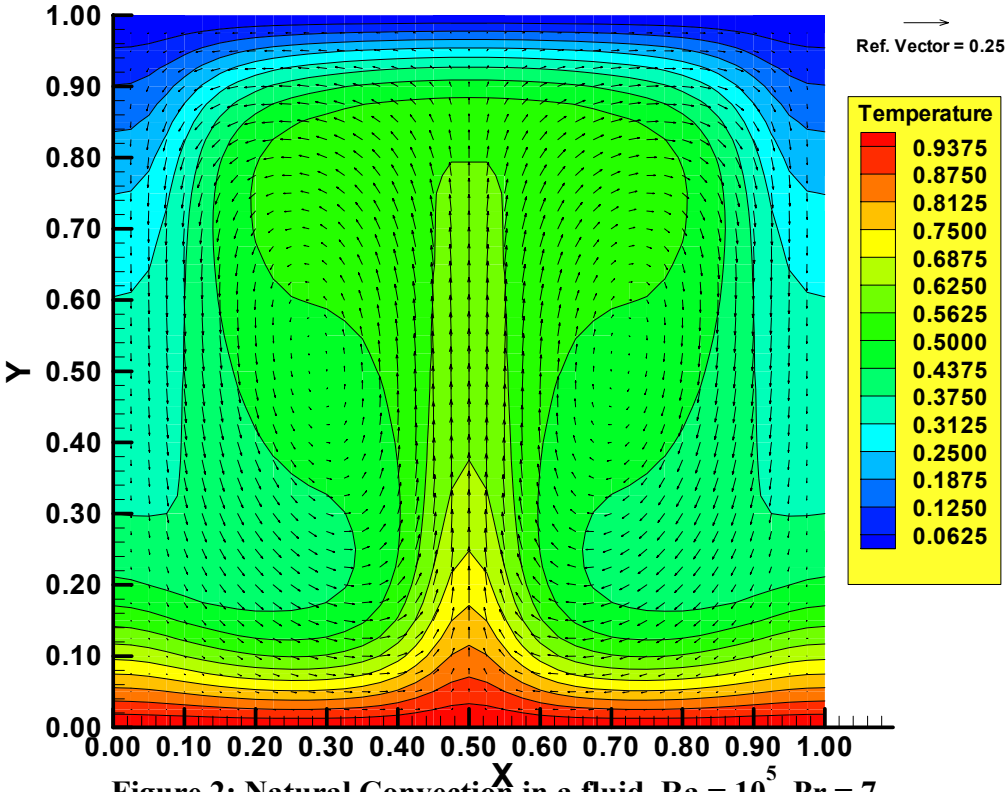

Figure 2: Natural Convection in a fluid, Ra = 10^5, Pr = 7.

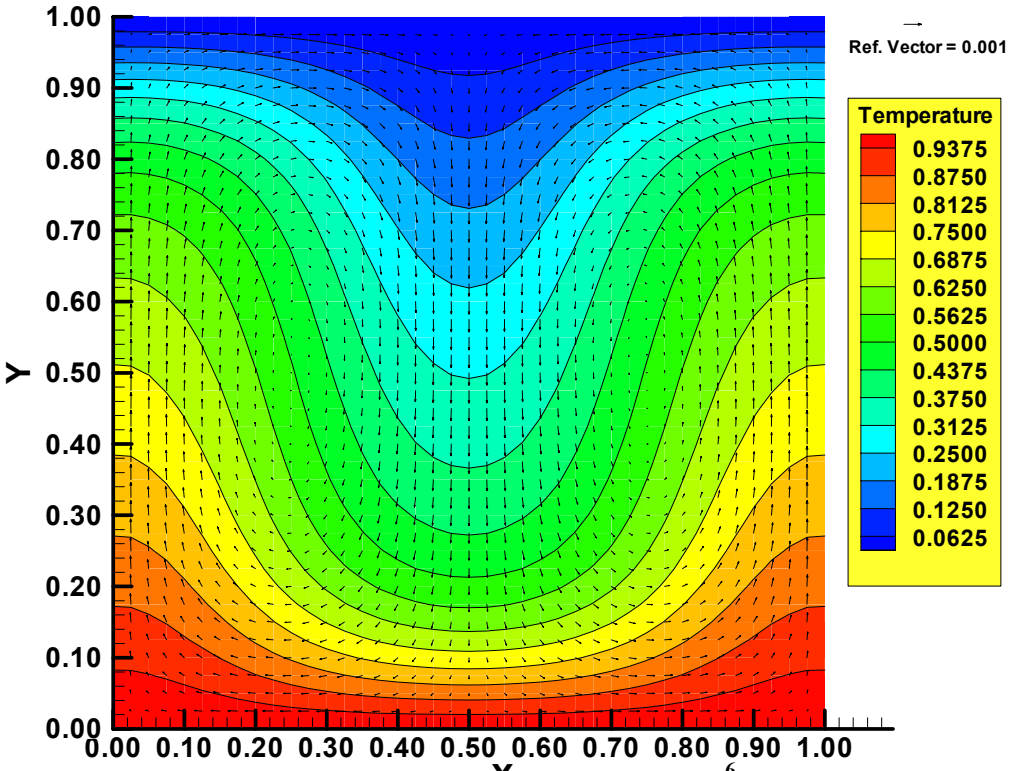

Figure 3: Natural Convection in Air, Ra = 10^6, Pr = 0.71.

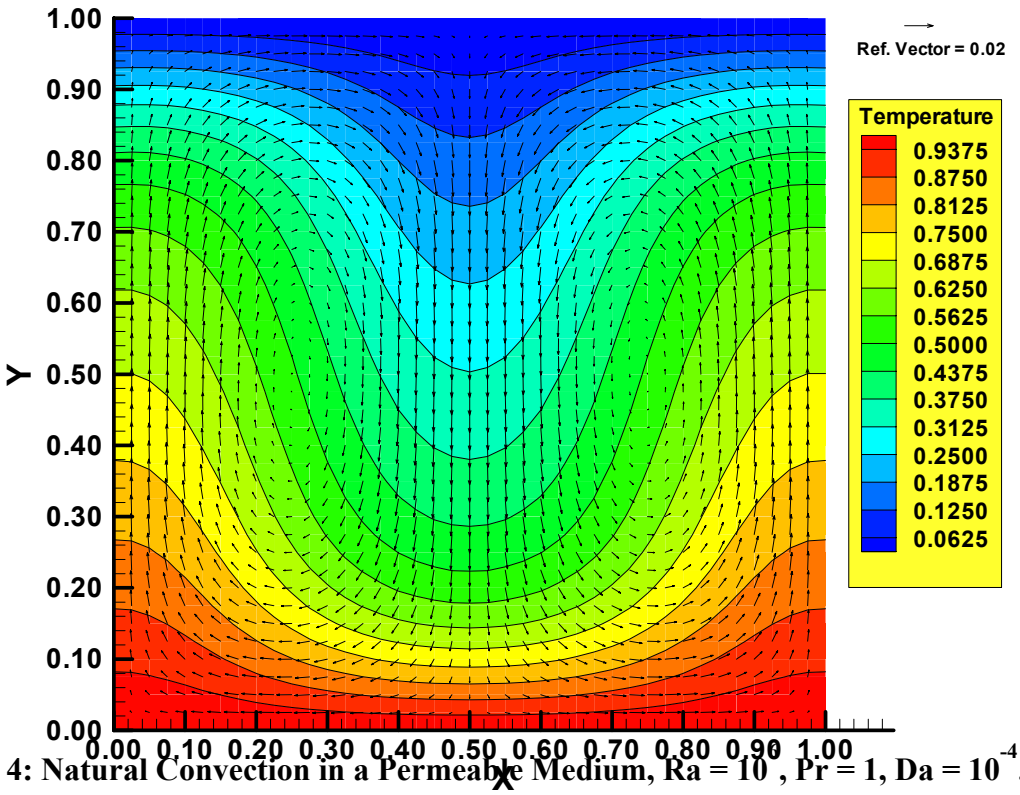

Figure 4: Natural Convection in a Permeable Medium, Ra = 10 , Pr = 1, Da = 10^{-4}.

Figure 5: Natural Convection in a Permeable Medium with Water as the Base Fluid. Ra = 10^{8}, Pr = 1, Da = 10^{-6}.

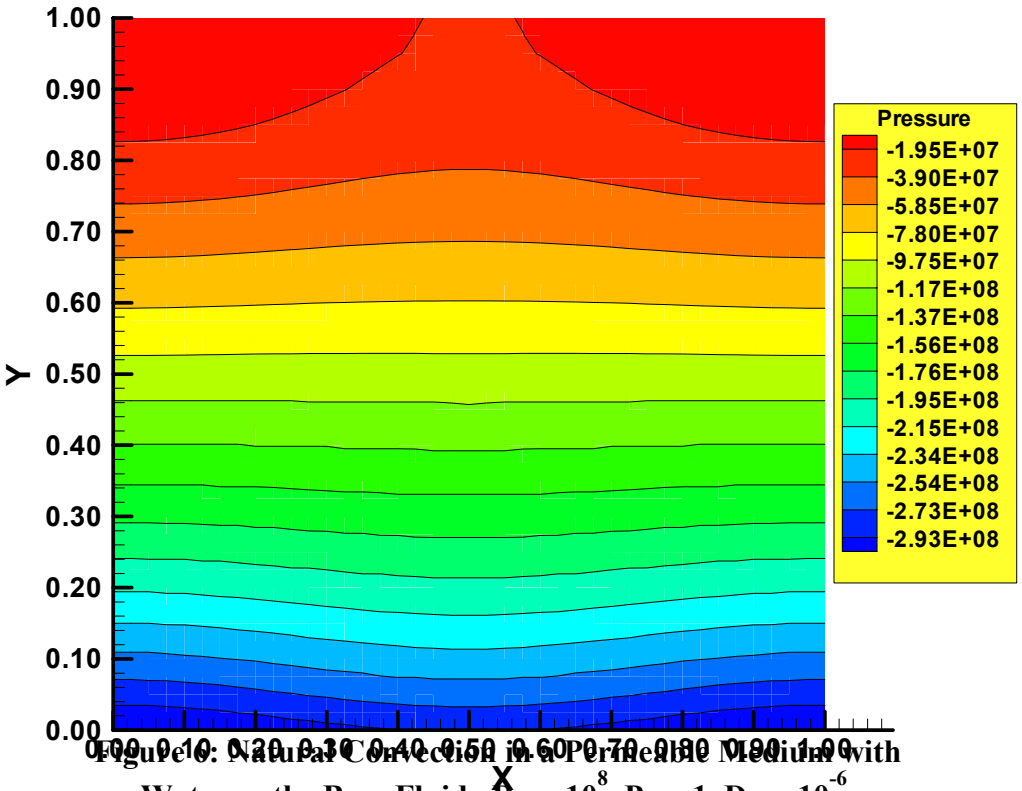

Figure 6: Natural Convection in a Permeable Medium with Water as the Base Fluid. Ra = 10^{8}, Pr = 1, Da = 10^{-6}.

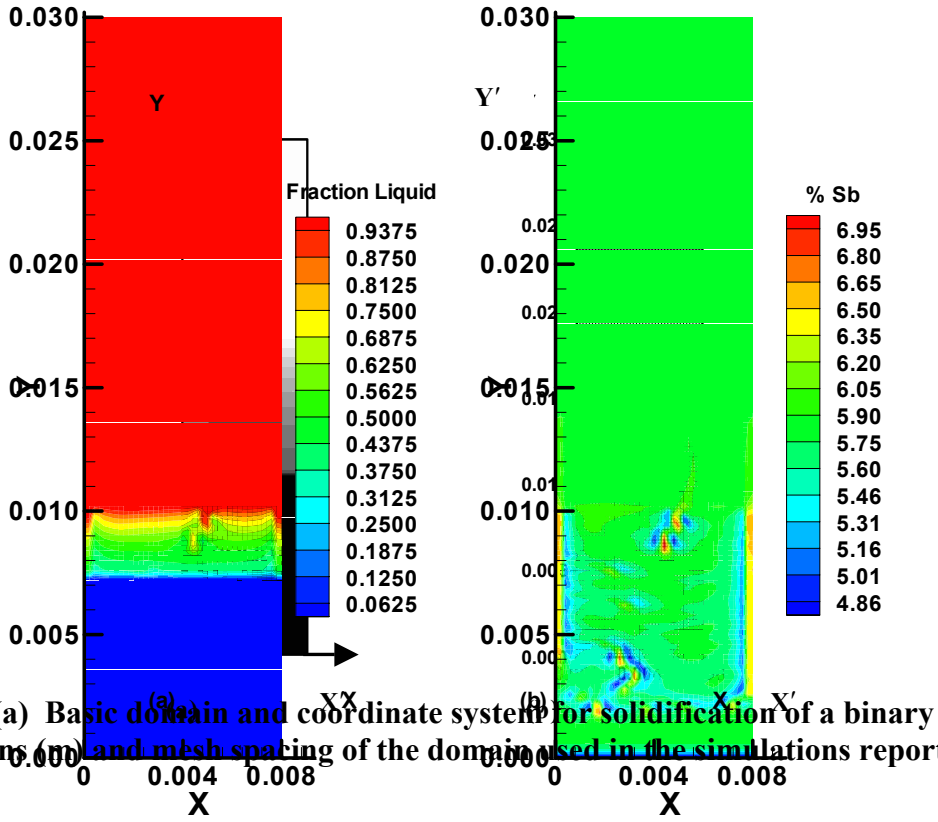

Figure 7. (a) Basic domain and coordinate system for solidification of a binary alloy. (b) Dimensions (m) and mesh spacing of the domain used in the simulations reported here.

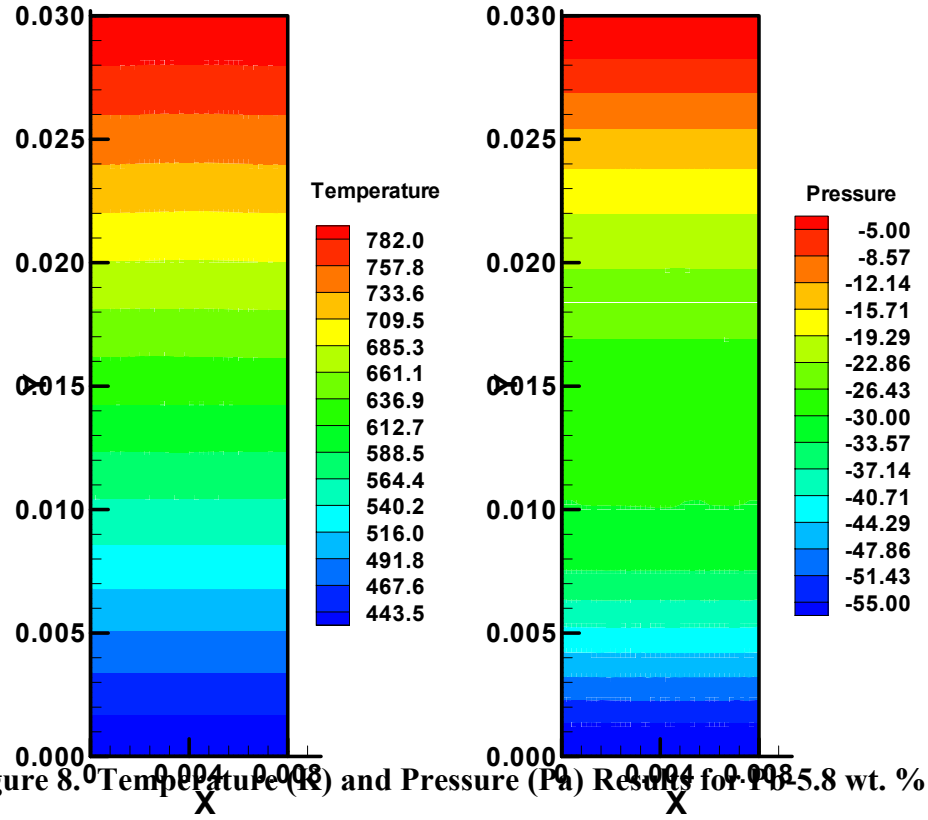

Figure 8. Temperature (K) and Pressure (Pa) Results for Pb-5.8 wt. % Sb.

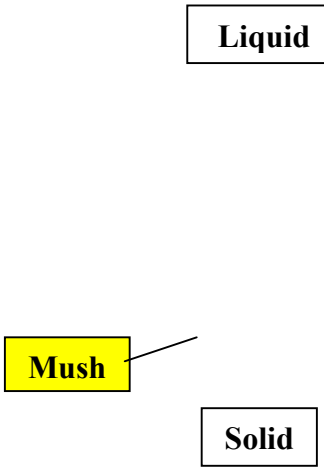

Figure 9. Fraction Liquid and Concentration Results for Pb-5.8 wt. % Sb.

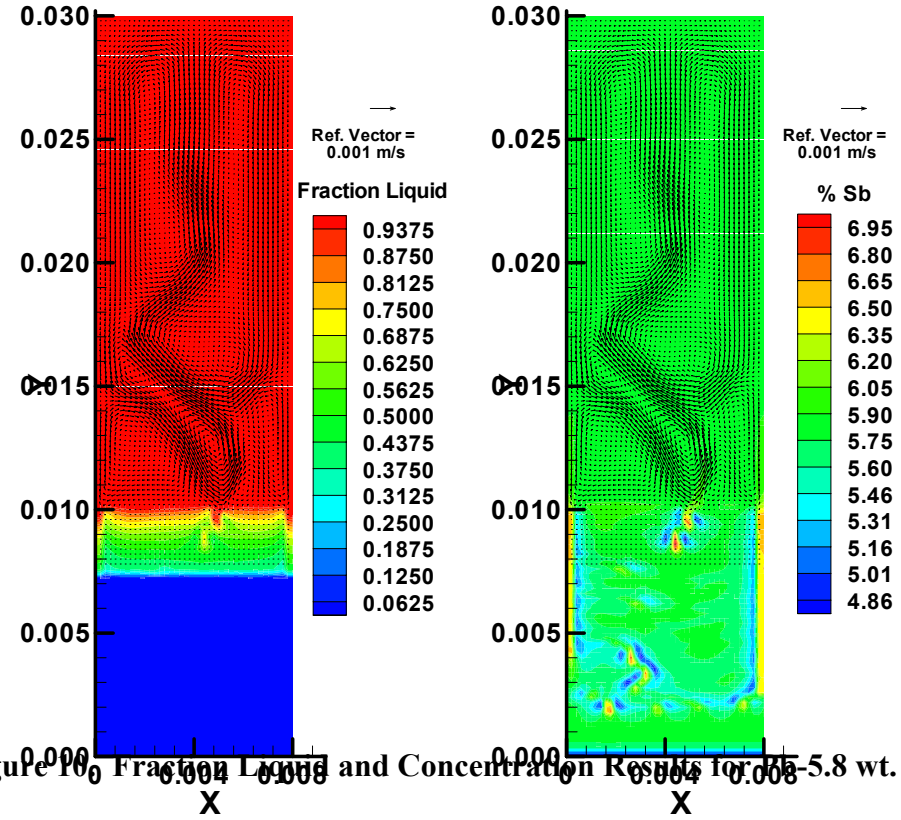

Figure 10. Fraction Liquid and Concentration Results for Pb-5.8 wt. % Sb.

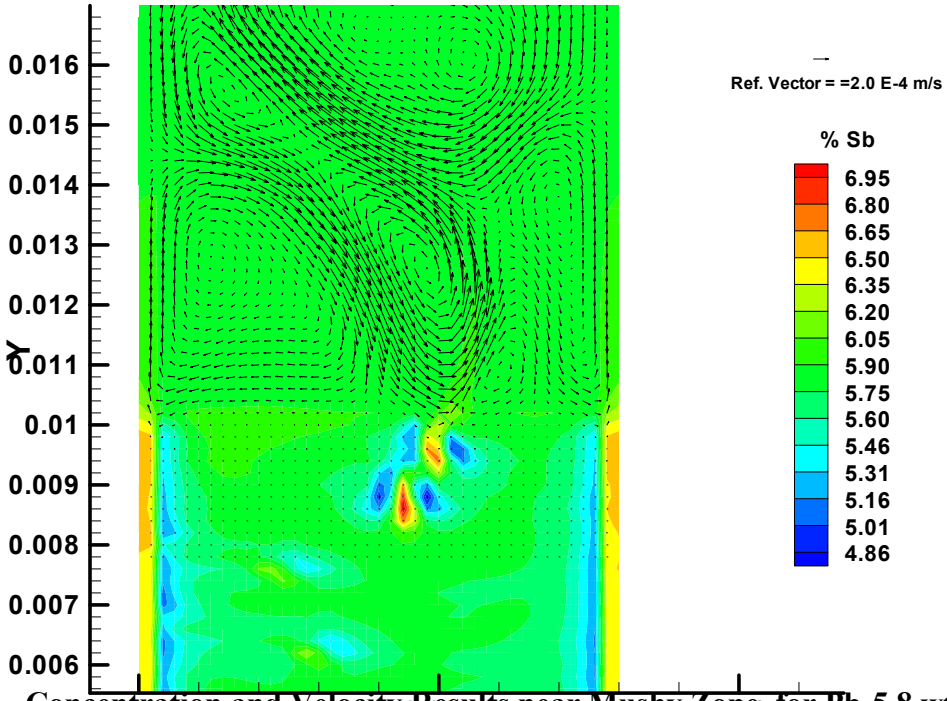

Figure 11. Concentration and Velocity Results near Mushy Zone, for Pb-5.8 wt. % Sb.

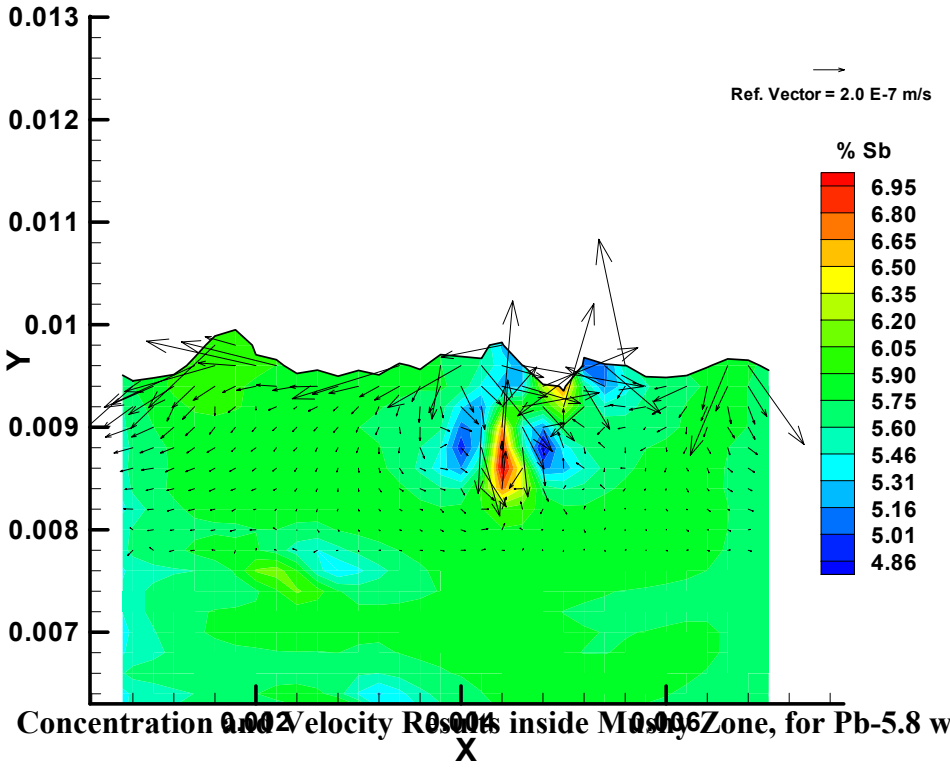

Figure 12. Concentration and Velocity Results inside Mushy Zone, for Pb-5.8 wt. % Sb.